Article

DNA Structural Distortions Induced by Ruthenium#Arene Anticancer Compounds

Christian Gossens, Ivano Tavernelli, and Ursula Rothlisberger

J. Am. Chem. Soc., **2008**, 130 (33), 10921-10928 • DOI: 10.1021/ja800194a • Publication Date (Web): 24 July 2008

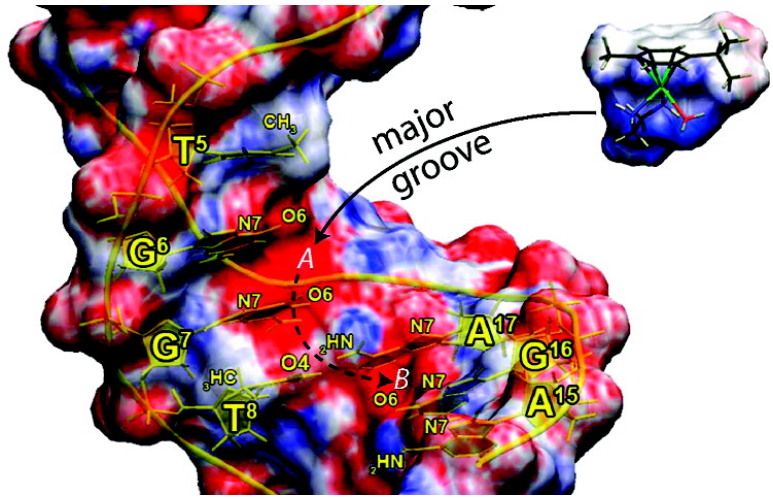

More About This Article

Additional resources and features associated with this article are available within the HTML version:

- Supporting Information
- Links to the 1 articles that cite this article, as of the time of this article download
- Access to high resolution figures
- Links to articles and content related to this article
- Copyright permission to reproduce figures and/or text from this article

View the Full Text HTML

Journal of the American Chemical Society is published by the American Chemical Society. 1155 Sixteenth Street N.W., Washington, DC 20036

J|A|C|S
ARTICLES

Published on Web 07/24/2008

DNA Structural Distortions Induced by Ruthenium−Arene Anticancer Compounds

Christian Gossens, Ivano Tavernelli, and Ursula Rothlisberger*

Laboratory of Computational Chemistry and Biochemistry, Institute of Chemical Sciences and Engineering, Ecole Polytechnique Fédérale de Lausanne, CH-1015 Lausanne, Switzerland

Received January 9, 2008; E-mail: ursula.roethlisberger@epfl.ch

Abstract: Organometallic ruthenium(II)−arene (RA) compounds combine a rich structural diversity with the potential to overcome existing chemotherapeutic limitations. In particular, the two classes of compounds [Ru(II)(η^6-arene)X(en)] and [Ru(II)(η^6-arene)$(X)_2$(pta)] (RA-en and RA-pta, respectively; X = leaving group, en = ethylenediamine, pta = 1,3,5-triaza-7-phosphaadamantane) have become the focus of recent anticancer research. *In vitro* and *in vivo* studies have shown that they exhibit promising new activity profiles, for which their interactions with DNA are suspected to be a crucial factor. In the present study, we investigate the binding processes of monofunctional RA-en and bifunctional RA-pta to double-stranded DNA and characterize the resulting structural perturbations by means of *ab initio* and classical molecular dynamics simulations. We find that both RA complexes bind easily through their ruthenium center to the N7 atom of guanine bases. The high flexibility of DNA allows for fast accommodation of the ruthenium complexes into the major groove. Once bound to the host, however, the two complexes induce different DNA structural distortions. Strain induced in the DNA backbone from RA-en complexation is released by a local break of a Watson−Crick base-pair, consistent with the experimentally observed local denaturation. The bulkier RA-pta, on the other hand, bends the DNA helix toward its major groove, resembling the characteristic DNA distortion induced by the classic anticancer drug cisplatin. The atomistic details of the interactions of RA complexes with DNA gained in the present study shed light on some of the anticancer properties of these compounds and should assist future rational compound design.

Introduction

The inorganic complex cisplatin, *cis*-[Pt$(NH_3)_2(Cl)_2$], is by far the most studied and widely used transition-metal drug in chemotherapy. However, its exact mechanism of action is still a matter of debate, even 50 years after its initial discovery.[1–3] It has been shown that cisplatin forms adducts with DNA, probably exerting its cytotoxic effect in this way.[4] X-ray and NMR structures of cisplatin bound to double-stranded DNA (dsDNA) reveal intrastrand cross-linking of adjacent guanine (G) bases (1,2-GG) as the major binding mode. This induces a bend of the DNA helix toward the major groove.[5,6] The bend is believed to be the basis for recognition by HMG proteins,[7] which in turn has been postulated to mediate the antitumor properties of the drug.[8]

While organometallic compounds are versatile and well-established tools in catalysis, the interest in their medicinal application dates only from 1979, when the antitumor activity of titanocene dichloride [$(Cp)_2$Ti$(Cl)_2$] was reported.[9,10] Despite the great clinical success of platinum compounds, the quest for designing improved drugs is still fueled by the poor selectivity and high toxicity of existing compounds and the occurrence of resistance against them. Recently, two organometallic ruthenium(II)−arene (RA) complexes of the general type [Ru(II)(η^6-arene)$(X)_2$(pta)][11] and [Ru(II)(η^6-arene)X(en)][12] (RA-pta and RA-en, respectively, where X = leaving group, en = chelating ethylenediamine, and pta = monodentate phosphine 1,3,5-triaza-7-phosphaadamantane) have emerged as promising antitumor compounds (Figure 1). These "piano stool" complexes share a π-bonded arene as the "seat of the stool", and various monodentate or chelating ligands occupy the remaining three coordination sites (the "legs"). Like cisplatin, RA complexes remain predominantly in their less reactive chloride form at high chloride concentrations (such as in blood plasma). At low chloride concentrations (e.g., inside a cell), they undergo aquation,[13,14] activating them toward reactions with biomolecules such as DNA and proteins.[14–19]

(1) Fuertes, M. A.; Alonso, C.; Pérez, J. M. *Chem. Rev.* **2003**, *103*, 645–662.
(2) Wang, D.; Lippard, S. J. *Nature Rev. Drug Discovery* **2005**, *4*, 307–320.
(3) Wong, E.; Giandomenico, C. M. *Chem. Rev.* **1999**, *99*, 2451–2466.
(4) Reedijk, J. *Chem. Commun.* **1996**, 801–806.
(5) Takahara, P. M.; Rosenzweig, A. C.; Frederick, C. A.; Lippard, S. J. *Nature* **1995**, *377*, 649–652.
(6) Gelasco, A.; Lippard, S. J. *Biochemistry* **1998**, *37*, 9230–9239.
(7) Ohndorf, U. M.; Rould, M. A.; He, Q.; Pabo, C. O.; Lippard, S. J. *Nature* **1999**, *399*, 708–712.
(8) Zhai, X.; Beckmann, H.; Jantzen, H. M.; Essigmann, J. M. *Biochemistry* **1998**, *37*, 16307–16315.
(9) Köpf, H.; Köpf-Maier, P. *Angew. Chem., Int. Ed. Engl.* **1979**, *18*, 477–478.
(10) Köpf-Maier, P.; Köpf, H. *Chem. Rev.* **1987**, *87*, 1137–1152.
(11) Allardyce, C. S.; Dyson, P. J.; Ellis, D. J.; Heath, S. L. *Chem. Commun.* **2001**, 1396–1397.
(12) Morris, R. E.; Aird, R. E.; Murdoch, P. d. S.; H.; Chen, J. C.; Hughes, N. D.; Parsons, S.; Perkin, A.; Boyd, G.; Jodrell, D. I.; Sadler, P. J. *J. Med. Chem.* **2001**, *44*, 3616–3621.

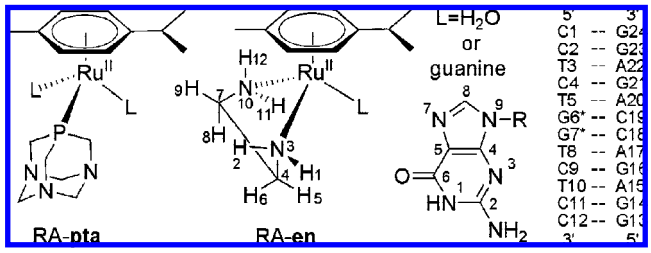

Figure 1. Structures and numbering of the ruthenium arene complexes RA-en (en = ethylenediamine) and RA-pta (pta = 1,3,5-triaza-7-phosphaadamantane)and the guanine ligand, and a schematic representation of the DNA sequence (asterisks indicate ruthenated site).

Like cisplatin, the RA-en compounds show strong cytotoxicity toward a broad spectrum of cancer cells. In addition, they were found to be active toward cisplatin-resistant cells.[20,21] In the presence of histidine, glutathione, cytochrome *c*, oligonucleotides, and DNA nucleobases [guanine (G), adenine (A), thymine (T), and cytosine (C)], the selectivity of RA-en for binding to guanine is nearly exclusive and exceeds that of cisplatin.[16,22,23] The ruthenium center binds to guanine N7 atoms, while its en ligand forms a hydrogen bond to the guanine O6 atom.[24] On the other hand, the RA-pta compounds display (*in vitro*) only modest cytotoxicity toward cancer cells and are nontoxic toward nontumorigenic cells. *In vivo* they were found to inhibit and reduce the weight of lung metastases and showed only mild effects on primary tumors and in general low overall toxicity.[25] Despite this wealth of information, a detailed atomistic knowledge of the effects of RA compounds on dsDNA is still lacking.

The most readily accessible electron donors of dsDNA are the N7 atoms of adenine and guanine. However, a theoretical rigid docking study for another organometallic complex, $[Cp_2Mo]^{2+}$, suggested that transition metal−arene compounds with two bulky ligands cannot bind to the major groove of dsDNA.[26] Nevertheless, experimental results obtained for RA-en and RA-pta suggest such binding,[14,27–29] and very recent NMR studies of an RA-en compound with a biphenyl ligand have confirmed this result.[30,31]

In the present study, we investigate the selectivity of RA-en toward guanine in dsDNA using explicit-solvent charge-neutralized molecular dynamics (MD) simulations. We also investigate the effects of RA-en and RA-pta binding on the local and the global structure of dsDNA. For our investigations, we use a quantum mechanical (QM) description for the RA complex and the coordinated guanine, and molecular mechanics (MM) to describe the rest of the DNA, the solvent, and the counterions, to give a hybrid QM/MM setup (Figures S1, S2). We used a model sequence of dsDNA comprised of two guanine bases at the center of a 12-mer in a B-type conformation, employed previously in a cisplatin study.[5] For the RA complexes we considered both benzene and *p*-cymene as arene ligands. This approach allowed for the description of local binding properties and chemical reactivity without tailored empirical parameters, and it also enabled us to develop specific force fields for the RA complexes. These tailor-made force fields gave excellent agreement with the QM/MM results, and so we performed long time-scale simulations to investigate the formation of global DNA structural distortions.

Methods and Computational Details

Isothermal−isobaric ensemble (NPT) classical MD simulations were performed using the AMBER 7&8 packages[38] with the parm99 force field.[39,40] The SHAKE algorithm was used to constrain bonds to hydrogen atoms. Additional parameters for the RA complexes were derived from DFT *in vacuo* calculations following the AMBER procedure. They were verified and further improved using a force-matching approach based on the QM/MM

(13) Wang, F.; Chen, H.; Parsons, S.; Oswald, I. D. H.; Davidson, J. E.; Sadler, P. J. *Chem. Eur. J.* **2003**, *9*, 5810–5820.
(14) Scolaro, C.; Bergamo, A.; Brescacin, L.; Delfino, R.; Cocchietto, M.; Laurenczy, G.; Geldbach, T. J.; Sava, G.; Dyson, P. J. *J. Med. Chem.* **2005**, *48*, 4161–4171.
(15) Wang, F.; Habtemariam, A.; van der Geer, E. P. L.; Fernandez, R.; Melchart, M.; Deeth, R. J.; Aird, R.; Guichard, S.; Fabbiani, F. P. A.; Lozano-Casal, P.; Oswald, I. D. H.; Jodrell, D. I.; Parsons, S.; Sadler, P. J. *Proc. Natl. Acad. Sci.U.S.A.* **2005**, *102*, 18269–18274.
(16) Wang, F.; Bella, J.; Parkinson, J. A.; Sadler, P. J. *JBIC, J. Biol. Inorg. Chem* **2005**, *10*, 147–155.
(17) Dorcier, A.; Dyson, P. J.; Gossens, C.; Rothlisberger, U.; Scopelliti, R.; Tavernelli, I. *Organometallics* **2005**, *24*, 2114–2123.
(18) Scolaro, C.; Geldbach, T. J.; Rochat, S.; Dorcier, A.; Gossens, C.; Bergamo, A.; Cocchietto, M.; Tavernelli, I.; Sava, G.; Rothlisberger, U.; Dyson, P. J. *Organometallics* **2006**, *25*, 756–765.
(19) (a) Colombo, M.; Gossens, C.; Tavernelli, I.; Rothlisberger, U. *From Enzymatic Catalysis to Anticancer Drugs: QM/MM Car−Parrinelllo Simulations of Biological Systems*; Special Volume: WATOC 2005; Royal Society of Chemistry: Cambridge, U.K., 2006; pp 85−100. (b) Gossens, C.; Tavernelli, I.; Rothlisberger, U. *Chimia* **2005**, *59*, 81–84.
(20) Aird, R. E.; Cummings, J.; Ritchie, A. A.; Muir, M.; Morris, R. E.; Chen, H.; Sadler, P. J.; Jodrell, D. I. *Br. J. Cancer* **2002**, *86*, 1652–1657.
(21) Guichard, S. M.; Else, R.; Reid, E.; Zeitlin, B.; Aird, R.; Muir, M.; Dodds, M.; Fiebig, H.; Sadler, P. J.; Jodrell, D. I. *Biochem. Pharmacol.* **2006**, *71*, 408–415.
(22) Chen, H.; Parkinson, J. A.; Morris, R. E.; Sadler, P. J. *J. Am. Chem. Soc.* **2003**, *125*, 173–186.
(23) Wang, F.; Xu, J.; Habtemariam, A.; Bella, J.; Sadler, P. J. *J. Am. Chem. Soc.* **2005**, *127*, 17734–17743.
(24) Gossens, C.; Tavernelli, I.; Rothlisberger, U. *J. Chem. Theory Comput.* **2007**, *3*, 1212–1222.
(25) Dyson, P. J.; Sava, G. *Dalton Trans.* **2006**, 1929–1933.
(26) Kuo, L. Y.; Kanatzidis, M. G.; Sabat, M.; Tipton, A. L.; Marks, T. J. *J. Am. Chem. Soc.* **1991**, *113*, 9027–9045.
(27) Novakova, O.; Chen, H.; Vrana, O.; Rodger, A.; Sadler, P. J.; Brabec, V. *Biochemistry* **2003**, *42*, 11544–11554.
(28) Novakova, O.; Kasparkova, J.; Bursova, V.; Hofr, C.; Vojtiskova, M.; Chen, H.; Sadler, P. J.; Brabec, V. *Chem. Biol.* **2005**, *12*, 121–129.
(29) Chen, H.; Parkinson, J. A.; Novakova, O.; Bella, J.; Wang, F.; Dawson, A.; Gould, R.; Parsons, S.; Brabec, V.; Sadler, P. J. *Proc. Natl. Acad. Sci. U.S.A.* **2003**, *100*, 14623–14628.
(30) Liu, H.-K.; Berners-Price, S. J.; Wang, F.; Parkinson, J. A.; Xu, J.; Bella, J.; Sadler, P. J. *Angew. Chem., Int. Ed.* **2006**, *45*, 8153–8156.
(31) Liu, L. H.-K.; Wang, F.; Parkinson, J. A.; Bella, J.; Sadler, P. J. *Chem. Eur. J.* **2006**, *12*, 6151–6165.
(32) Laio, A.; VandeVondele, J.; Rothlisberger, U. *J. Chem. Phys.* **2002**, *116*, 6941–947.
(33) Laio, A.; VandeVondele, J.; Rothlisberger, U. *J. Phys. Chem. B* **2002**, *106*, 7300–7307.
(34) Takahara, P. M.; Frederick, C. A.; Lippard, S. J. *J. Am. Chem. Soc.* **1996**, *118*, 12309–12321.
(35) Jamieson, E. R.; Lippard, S. J. *Chem. Rev.* **1999**, *99*, 2467–2498.
(36) Gossens, C.; Dorcier, A.; Dyson, P.; Rothlisberger, U. *Organometallics* **2007**, *26*, 3969–3975.
(37) Perez, A.; Marchan, I.; Svozil, D.; Sponer, J.; Cheatham, T. E.; Laughton, C. A.; Orozco, M. *Biophys. J.* **2007**, *92*, 3817–3829.
(38) Case, D. A.; Pearlman, D. A.; Caldwell, J. W.; Cheatham, T. E., III; Wang, J.; Ross, W. S.; Simmerling C. L.; Darden, T. A.; Merz, K. M.; Stanton, R. V.; Cheng, A. L.; Vincent, J. J.; Crowley, M.; Tsui, V.; Gohlke, H.; Radmer, R. J.; Duan, Y.; Pitera, J.; Massova, I.; Seibel, G. L.; Singh, U. C.; Weiner, P. K.; Kollman, P. A. *AMBER 7*; University of California: San Francisco, 2002.
(39) Cornell, W. D.; Cieplak, P.; Bayly, C. I.; Gould, I. R.; Merz, K. M.; Ferguson, D. M.; Spellmeyer, D. C.; Fox, T.; Caldwell, J. W.; Kollman, P. A. *J. Am. Chem. Soc.* **1995**, *117*, 5179–5197.
(40) Cheatham, T. E., III; Cieplak, P.; Kollman, P. A. *J. Biomol. Struct. Dyn.* **1999**, *16*, 845–862.

trajectories (Figures S9−S13, Tables S1−S18).[41] We used both canonical B-DNA (generated with the AMBER module *nucgen*) and the DNA crystal structure of a cisplatin adduct to DNA (PDB entry 1AIO) as starting configurations for our simulations.[5,34] As reference calculations, the same DNA structure (without any drug) and canonical B-DNA were simulated. The systems were hydrated with explicit TIP3P water molecules and neutralized with counterions (20 Na^+). The box dimensions were chosen to achieve a minimum distance of 20 Å between two periodically replicated images of the DNA, resulting in a typical fundamental cell of ∼45 × 50 × 60 $Å^3$ with about 4300 water molecules. The systems were simulated with a time step of 1−1.5 fs and were maintained at 310 K and 1 atm by Berendsen baro- and thermostats. Electrostatic interactions were treated by the particle-mesh Ewald (PME) method.

The QM part of the QM/MM calculations comprising the ruthenium compounds and the coordinated guanine molecule(s) was described at the DFT/BLYP level using the CPMD program.[42−44] The MM part was treated using the force field described above. Car−Parrinello dynamics[45] were performed using a plane-wave energy cutoff of 75 Ry, a time step of 0.097 fs, a fictitious electron mass of 400 au, and a temperature of 310 K (maintained by a Nosé-Hoover thermostat). An analytical local pseudopotential (PP) for hydrogen atoms and nonlocal, norm-conserving PPs of the Martins−Trouiller type[46] for all other elements were used (electrons up to the 1s shell for C, N, and O, up to 2p for P, and up to 3d for Ru were considered in the core).[17] The semicore PP for Ru incorporates scalar relativistic effects. Integration of the nonlocal parts of the PPs was obtained via the Kleinman−Bylander scheme[47] for all of the atoms, whereas for Ru the PP was integrated numerically using a Gauss−Hermite quadrature. The interaction between the MM and the QM parts was described by a fully Hamiltonian hierarchical coupling scheme.[32,33] A similar setup has yielded good results for cisplatin/DNA interactions[48] and bleomycin.[49]

Structural properties of the DNA were calculated using the program Curves 5.3. For the global bending angle, a method described by Lankas et al. was employed.[50] Two base-pairs on every side of the 12-mer were omitted for the calculations of the helical axis. For setups of RA-pta, the reference plane is an average plane located between G6-C19/G7-C18.

The calculation of the free energy profile along a reaction coordinate (a bond distance in our case) was performed following the standard procedure.[51] In the MD simulation, the distance constraint was maintained via a Lagrangian multiplier, λ, and the free energy profile was then constructed from

$$\Delta F(R) = -\int_{R_{\min}}^{R_{\max}} \mathrm{d}R' \langle \lambda \rangle_{R'}^{\mathrm{cond}}$$

where $\Delta F(R)$ denotes the relative free energy as a function of the bond length. $\langle \lambda \rangle_{R'}^{\mathrm{cond}}$ is the conditional average of the Lagrange multiplier with the constrained coordinate fixed at the value R',

$$\langle \lambda \rangle_{R'}^{\mathrm{cond}} = \frac{\int \mathrm{d}^N p\, \mathrm{d}^N r\, \lambda(r,p)\, \mathrm{e}^{-\beta H(r,p)}\, \delta(R(r) - R')}{\int \mathrm{d}^N p\, \mathrm{d}^N r\, \mathrm{e}^{-\beta H(r,p)}\, \delta(R(r) - R')}$$

where r and p denote the collective coordinates and momenta of the system, $H(r,p)$ is the N-particle total Hamiltonian ($H = H_{\mathrm{QM}} + H_{\mathrm{MM}} + H_{\mathrm{QM/MM}}$), and $\beta = 1/k_{\mathrm{B}}T$.

List of Performed Simulations. In this study, we made use of different simulation techniques and setups. In order to facilitate the discussion of the results, we report here a complete list of the most relevant simulations preformed, together with the corresponding simulation conditions. In total, we performed seven classical MD simulations [Cl.1−7], four QM/MM MD runs [Qm.1−4], and two long sets of combined simulations for the characterization of the defect formation upon drug binding to DNA [Df.1−2].

[Cl.1]. Classical MD simulation of B-DNA. Equilibration run at 300 K for 50 ns. The initial configuration was generated with the AMBER module *nucgen*.

[Cl.2−4]. Classical MD simulations for the docking of RA-en to B-DNA. We performed three independent runs of 20 ns each. The initial configurations were taken randomly from the trajectory [Cl.1], and the [Ru(η^6-cymene) (en)]$^{2+}$ moiety was placed about 20 Å away from the central GC base-pair. In the first two simulations, the RA-en was placed facing the major groove, and in the third, it was facing the minor groove.

[Cl.5]. Classical MD reference simulation of the cisplatin−DNA complex. The simulation was carried out for 25 ns. At the end of the run, the drug was removed and the DNA went back to the normal B-DNA configuration within 5 ns.

[Cl.6]. Classical MD simulation of the RA-pta−DNA adduct. The starting structure was generated from the cisplatin−DNA adduct [Cl.5] after replacement of the drug with RA-pta. In the case of the *p*-cymene compound, the simulation involved a long equilibration run of 35 ns. From this trajectory, we extracted a frame in configuration I (see Figure 5B, below), and after replacement of *p*-cymene with benzene, we computed a second classical MD trajectory of 35 ns.

[Cl.7]. Classical simulation of the protonated RA-pta compound [Ru(η^6-benzene)(pta-H^+)]$^{3+}$ docked to DNA. The starting configuration was taken from the QM/MM trajectory [Qm.3]. The simulation was carried out for 20 ns.

[Qm.1]. QM/MM simulation for the calculation of the free-energy profile for RA-en binding to DNA. The quantum system consists of the guanine G6, [Ru(η^6-cymene)(en)]$^{2+}$, and five water molecules. The starting structure was taken from the classical run [Cl.2]. The calculation of the complete thermodynamic free energy profile required (i) an initial unconstrained QM/MM run of 1 ps, (ii) a series of 26 thermodynamic integration steps along the Ru−N7 reaction coordinate, and (iii) a series of 20 thermodynamic integration steps along the Ru−OH_2 reaction coordinate. Depending on the convergence of the constraint force, each step in the thermodynamic integration required from 1 to 5 ps simulation time.

[Qm.2]. QM/MM run for the study of the binding mode of RA-en. The quantum system consists of guanine G6 and the RA-en complex. The starting structure was obtained from a classical MD run of 10 ns, in which the interaction between the Ru atom and the atom N7 of the guanine was modeled with a classical potential (see Tables S2−S18). The QM/MM simulation was carried out for 50 ps.

[Qm.3]. QM/MM study of the binding mode of RA-pta. The quantum system consists of the guanines G6 and G7 and the [Ru(η^6-benzene)(pta)]$^{2+}$ complex. The starting configuration was taken from the trajectory computed in [Cl.4]. The system was simulated for 15 ps.

[Qm.4]. Same setup and conditions as in [Qm.3] but for the complex [Ru(η^6-cymene)(pta)]$^{2+}$.

[Df.1]. Classical and QM/MM MD simulations for the study of RA-pta-induced DNA bending. Starting from six different structures in configuration I (Figure 5B) obtained in [Qm.3], we computed six independent classical trajectories of 22 ns each. Among them, three are computed with the compound [Ru(η^6-benzene)(pta)]$^{2+}$ and the other three with [Ru(η^6-cymene)(pta)]$^{2+}$. For configuration

(41) Maurer, P.; Laio, A.; Hugosson, H. W.; Colombo, M.; Rothlisberger, U. *J. Chem. Theory Comput.* **2007**, *3*, 628–639.
(42) *CPMD*; IBM Corp./Max Planck Institute: Stuttgart, 2006.
(43) Becke, A. D. *Phys. Rev. A* **1988**, *38*, 3098–3100.
(44) Lee, C.; Yang, W.; Parr, R. G. *Phys. Rev. B* **1988**, *37*, 785–789.
(45) Car, R.; Parrinello, M. *Phys. Rev. Lett.* **1985**, *55*, 2471–2474.
(46) Troullier, N.; Martins, J. L. *Phys. Rev. B* **1991**, *43*, 1993–2006.
(47) Kleinman, L.; Bylander, D. M. *Phys. Rev. Lett.* **1982**, *48*, 1425–1428.
(48) Spiegel, K.; Rothlisberger, U.; Carloni, P. *J. Phys. Chem. B* **2004**, *108*, 2699–2707.
(49) Karawajczyk, A.; Gossens, C.; Rothlisberger, U.; Buda, F. *J. Phys. Chem. B* **2006**, *110*, 21245–21250.
(50) Lankas, F.; Sponer, J.; Hobza, P.; Langowski, J. *J. Mol. Biol.* **2000**, *299*, 695–709.
(51) Frenkel, D.; Smit, B. *Understanding Molecular Simulation*; Academic Press: San Diego, CA, 2002.

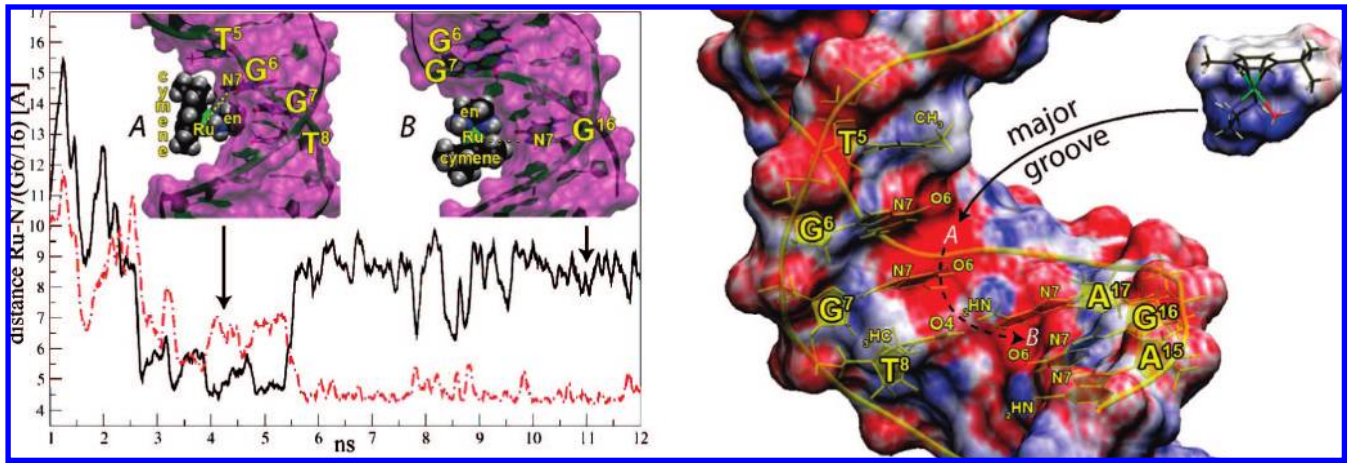

Figure 2. The RA-en compound enters the B-DNA major groove in an unconstrained MD run first at site A and then at site B. The graph shows the distances of the ruthenium to the N7 of G6 (black line) and G16 (red dashed line), respectively (solvent-accessible surface in purple, RA-en in vdW representation). The electrostatic potential (ESP, right panel) was calculated for the DNA 12-mer (classical) and for the aqua species of RA-en (QM) and mapped on the solvent-accessible surfaces (red = negative, blue = positive). Two regions in the major groove (around G6/G7 and around G16) are highly negatively charged. In contrast, a relatively low negative ESP is measured around the backbone phosphates. The RA-en complex carries a total charge of 2+ and is therefore attracted by the negative ESP of the polyanionic DNA. The *p*-cymene and in particular its methyl groups are the least positive regions of the compound, whereas the en and aqua ligands exhibit the strongest positive ESP.

II (Figure S5), we performed a single 22 ns long classical MD simulation, followed by a QM/MM MD simulation of about 4 ps.

[Df.2]. Classical and QM/MM MD simulations for the study of RA-en-induced DNA bending. Starting from different structures obtained from the trajectory in [Qm.2], we performed two independent 20 ns long trajectories [Df.2a,b]. An additional trajectory using a modified Amber force field with improved dihedral angle parametrization was also computed [Df.2c].

Results and Discussion

Migration of RA-en toward Guanine in the Major Groove. The high affinity of RA-en toward the N7 atom of guanine, N7(G),[22] intuitively suggests a preference for DNA major groove binding of the RA compounds (as observed for cisplatin). However, experiments have also shown evidence for minor groove interactions.[27] In order to address this contention, we performed three classical MD simulations of 15 ns each [Cl.2−4], in which we placed the [Ru(η^6-cymene)(en)]$^{2+}$ moiety approximately 20 Å away from the two central GC base-pairs (Figures 2, 3, S3). In two of the simulations, the RA-en was initially placed facing the major groove, and in the third, it was placed facing the minor groove. Our results show that (i) RA-en can easily accommodate itself in the major groove of dsDNA and (ii) the compound exhibits a strong selectivity for guanine in GC-rich sequences of B-DNA. We observed some minor groove interactions, but they would not allow for a reaction with N7(G) (Figure 3). In all three simulations, the charged [Ru(η^6-cymene)(en)]$^{2+}$ complex preferred close interactions with the polyanionic DNA over solvation by bulk water. The en moiety plays a key role in this recognition process. In one of the simulations, RA-en enters the major groove and docks with its en moiety to the guanines G6 and G7 of the central GC pairs (see Figure 2, site A).

In the resulting adduct A, the ruthenium comes within 4 Å of the putative DNA-binding atom N7(G6), which is in the range of a coordinative binding distance. Moreover, characteristic hydrogen bonds to the guanine O6 atom, O6(G6), and van der Waals (vdW) contacts with adjacent bases are already established (details are given below). Throughout our simulations, the hydrophobic arene points toward bulk water (like an open

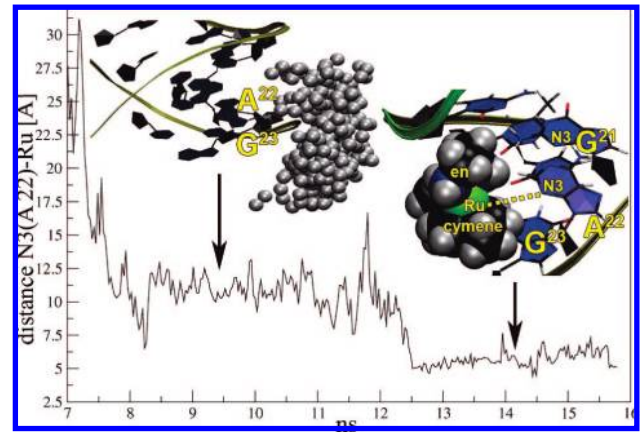

Figure 3. Starting at a distance of 15 Å from the N3(G6) located at the central minor groove, RA-en migrates through the bulk water until it undergoes metastable interactions via its en moiety with the DNA backbone between the phosphates of A22 and G23. The figure shows the distribution of the (en)NH_2 hydrogen (silver balls) during this part of the simulation. The RA-en complex fluctuates around this position for ∼4 ns, until it finally enters with its en moiety into the minor groove at A22 and G21, where it remains for the rest of the simulation.

umbrella). It appears that this orientation may help maintain attachment to the DNA by hindering the resolvation of the en moiety. After approximately 3 ns, RA-en escapes from binding site A and moves along the DNA surface two base-pairs farther along in the DNA sequence (Figure 1), where it is attracted by another guanine (G16) on the complementary strand (see Figure 2, site B). Also in this configuration, the above-mentioned hydrogen bond to the O6(G16) is formed.

The higher flexibility at the end of the model 12-mer DNA reduces the steric hindrance of the bulky *p*-cymene group, which probably explains why the compound prefers G16 over the central G6/G7 pair. Not surprisingly, as shown in Figure 2, the preferred docking sites observed in our classical MD simulations are those with a highly negative electrostatic potential (ESP). The strong positive ESP of the charged [Ru(η^6-cymene)-(H_2O)(en)]$^{2+}$ suggests that the observed regio-selectivity is driven by long-range electrostatic attractions. Once the RA-en

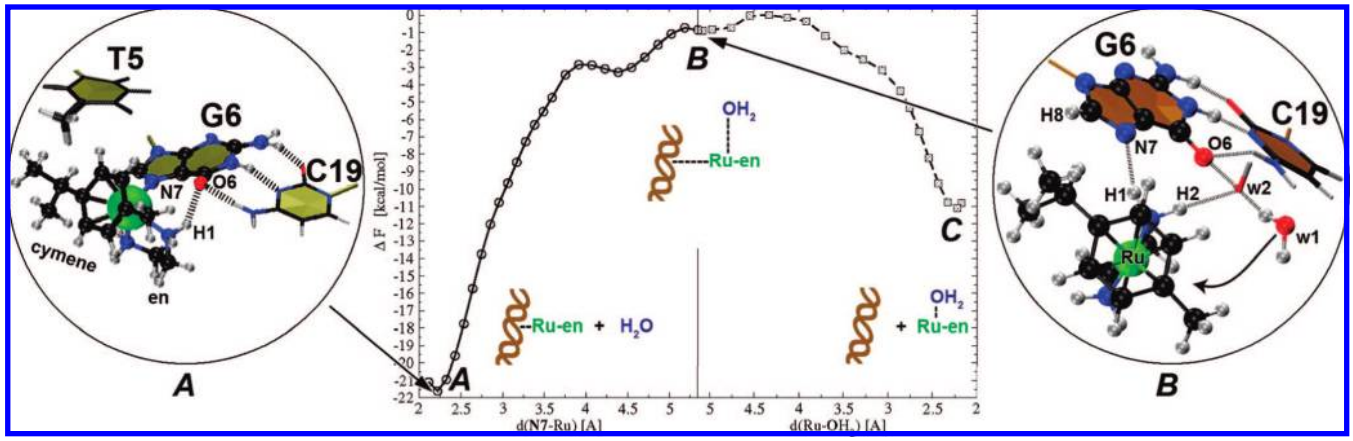

Figure 4. Free energy profile for the two-step reaction of $[Ru(p\text{-cymene})(H_2O)(en)]^+$ with the N7 of guanine in DNA, obtained by thermodynamic integration using QM/MM simulations (total sampling time 56 ps). Inlay A shows a snapshot of our MD trajectory in which the ruthenium complex binds to the guanine-N7 in the DNA major groove. Snapshot B shows the partially solvated, transition-state-like, under-coordinated T-shaped ruthenium complex at Ru−N7 = 5.35 Å. Once the strong H-bond between the en moiety and O6(G6) is broken, the en-H1 slides along G6 and forms a new H-bond with N7(G6). The structural water w2 bridges the en moiety of RA-en to O6(G6), while the en-N*H1* forms a H-bond to N7(G6). Solvent water molecules, counterions, and DNA have been omitted for clarity. Atoms depicted as spheres are treated at the QM level of theory.

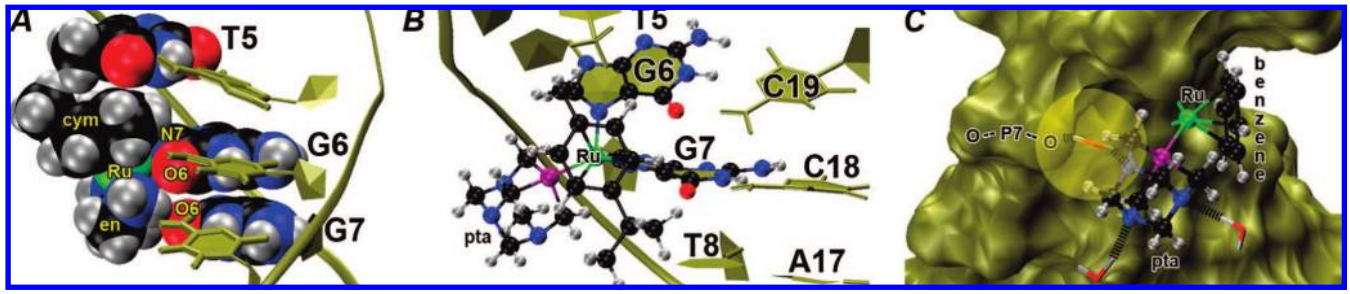

Figure 5. Representative snapshots from QM/MM MD simulations. (A) Monofunctional RA-en bound to G6 (seen from complementary strand; QM system as in Figure 4). The en-N*H1*−O6 hydrogen bond is quite strong, as becomes evident from a length of H1−O6 = 2.34 ± 0.38 Å and a $N_{en}-H_{en}-O_6$ angle of 131 ± 20°. Remarkably, the same en-N*H1* hydrogen also exhibits a strong H-bond (2.45 ± 0.42 Å, 132 ± 16°) to the O6 of G7 at the same time. (B) Bifunctional $[Ru(\eta^6\text{-}p\text{-cymene})(pta)]^{2+}$ bound to G6/G7 of DNA with its methyl group partially inserted between T5 and G6. (C) Bifunctional $[Ru(\eta^6\text{-benzene})(pta)]^{2+}$ bound to G6/G7 of DNA (seen from the bulk water; solvent-accessible surface shown). The classical water solvates the pta ligand, while a "structural" water molecule forms a H-bond bridge with an oxygen in phosphate 7.

is close to the guanine, short-range chemoselective H-bonds to the O6(G) and vdW interactions of the *p*-cymene (i.e., thymine methyl groups) dictate the final orientation.

Free Energy Profile for RA-en Binding to Guanine in DNA. The unconstrained classical MD docking study allowed us to sample the configurational space of the system over extended periods of time (tens of nanoseconds). In order to obtain further insight into the covalent binding of $[Ru(\eta^6\text{-cymene})(H_2O)(en)]^{2+}$ to the N7 of G6, we employed a hybrid QM/MM MD scheme [Qm.1]. In this approach, the region of chemical interest, which comprises G6, $[Ru(\eta^6\text{-cymene})(en)]^{2+}$, and the five closest H_2O molecules, is treated using density functional theory (DFT/BLYP). The remaining part of the system is coupled to the QM region[32,33] and treated using a classical force field. In this way, we can obtain a free energy profile for the reaction of RA-en with DNA by using a thermodynamic integration of the average constraint force along selected reaction coordinates (Figure 4).

An initial unconstrained QM/MM MD run of 1 ps confirmed the stability of the $[Ru(\eta^6\text{-cymene})(en)]^{2+}$ moiety in the docking site found by the classical MD study. During this simulation, the compound neither binds spontaneously to the G6 nor gets expelled from the binding site.

However, the $[Ru(\eta^6\text{-cymene})(H_2O)(en)]^{2+}$ complex may approach the N7 of G6 via either its aqua ligand or the en ligand. Therefore, we investigated first the binding reaction starting from state A in Figure 2 to obtain the well-defined RA-en−DNA adduct (Figures 4A, 5A). From this structure, we followed subsequently the detachment reaction toward the free aqua complex (state C in Figures 4 and S4). In this way, the ruthenium center was free to react with any surrounding water molecules during the dissociation process.

Binding to N7(G6). A constrained MD run was started from the equilibrated structure shown in Figure 2A, for which the Ru−N7(G6) distance was decreased from 4.40 Å to 2.12 Å in intervals of ∼0.1 Å (Figure 4). As a consequence, the RA-en compound moved toward G6, while G6 slid below T5 in the direction of the ruthenium compound, thereby optimizing T5/G6 $\pi-\pi$ stacking. This movement of G6 was transferred to phosphates 6 and 7 of the same strand, introducing a localized S-shaped distortion in the backbone of the ruthenated strand. The resulting binding mode was stabilized by three key interactions that we observed in all our simulations [Cl.2−4, Qm.2]: (i) the ruthenium coordination to N7(G6); (ii) a strong hydrogen bond between en-N*H1* and O6(G6), without perturbation of the Watson−Crick (WC) hydrogen bonds between G6 and C19 (Figure 4A); and (iii) attractive vdW interactions of the *p*-cymene moiety with the aromatic moiety and the methyl group of T5. As a result, G6 literally chelates the RA-en compound with its N7 and O6 atoms. The corresponding gain

in free energy is of the order of 20 kcal/mol and indicates that N7 coordination is highly preferred over a solvated, formally under-coordinated RA-en complex like that observed near the transition state (Figure 4B).

Detachment from DNA. We also studied the detachment of RA-en starting from the bound state obtained in the previous step [Qm.1]. Using thermodynamic integration, we increased the Ru−N7 distance up to 5.35 Å, allowing ligand exchange of N7(G6) with H_2O. With increasing Ru−N7 distance, G6 moves back toward its original B-DNA position, thereby relaxing the backbone strain that was introduced during the binding phase. The en-H1 slides along G6 (Figure 4B) and forms a new H-bond with N7(G6), while O6(G6) remains connected to RA-en via the formation of a stable water bridge (O6−w2−en-H2). Although the ruthenium center is formally under-coordinated and some water oxygen atoms come as close as 3.9 Å, no reactions with the surrounding QM water molecules take place on the time scale of our simulations (46 ps). This is most likely because the bulky arene and en moieties prevent direct access to the ruthenium. For Ru−N7 distances less than 3.75 Å, all water oxygens that come closer than 4.0 Å to the ruthenium center approach from the back side of the en ligand. At even longer Ru−N7 distances, the en moiety turns relative to the G6 orientation, and the ruthenium center becomes also accessible to water molecules approaching from the region close to H8 of G6 (bulk water side, Figure 4B). However, the large majority of water molecules still approach the ruthenium center from the back side.

After releasing the Ru−N7 constraint at 5.35 Å, we observe rupture of the en-N*H1*−N7 hydrogen bond and a migration of RA-en toward the bulk water within 0.3 ps, which results in a complete solvation of the formally under-coordinated compound. Again, however, no spontaneous coordination of a solvent H_2O to RA-en occurs. The long lifetime of the formally under-coordinated $[Ru(\eta^6\text{-cymene})(en)]^{2+}$ moiety justifies the exclusion of the coordinated H_2O during the initial classical migration study and might suggest a dissociative mechanism for the reaction of Ru−N7(DNA) to Ru−OH_2.

Solvation of the RA-en Moiety and Its Reaction with H_2O. To determine the free energy changes involved in the reaction of RA-en with a water molecule, we applied again a constrained MD-based thermodynamic integration scheme. In this case, the Ru−N7 distance was kept constant at 5.35 Å, and a new distance constraint, between the ruthenium and the oxygen of water w1, was introduced (Figure 4B). In all previous MD simulations, this water molecule stayed close to the ruthenium center (<6.5 Å) and several times came as close as 3.9 Å. Moreover, it does not interact with either the isopropyl or the methyl group of the *p*-cymene ligand. As is apparent from Figure 4, the reaction to form the RA-en aqua species has an activation free energy barrier of only ∼1.0 kcal/mol. Although the barrier is small, we did not observe the water reacting with the ruthenium center on the time scale of our unconstrained QM/MM simulations.

The computed free energy profile (Figure 4) shows a gain of 11 kcal/mol from binding the hydrolyzed compound to DNA. We computed activation free energies of 11 kcal/mol for the reaction of $[Ru(p\text{-cymene})(H_2O)(en)]^+$ with the N7 of guanine in DNA and 21 kcal/mol for the detachment of the $[Ru(p\text{-cymene})(en)]^{2+}$ moiety.

DNA Binding Mode of RA-en. In order to gain further insight into the properties of the binding site, we performed 50 ps of QM/MM MD simulations. The QM region consisted of RA-en and G6, and we began from a classically equilibrated structure [Qm.2]. The simulations showed that there is a preference for the cymene ligand to become oriented toward T5 (5′-direction) and the en ligand toward G7 (3′-direction) of the ruthenated DNA strand (relative to the Ru−N7 bond at G6; Figure 5A). Reversing the orientation of the ligands was shown to be unstable using classical MD. In this case, the aromatic cymene hydrogen atoms and parts of the aromatic system are partly intercalated into the space between T5 and G6. As a consequence, the rise between T5 and G6 is increased by on average 0.6 Å compared to B-DNA. Besides this rearrangement, G6 remains at its original B-DNA position. It appears that the compound prefers this local orientation due to the above-mentioned characteristic H-bonds to O6 atoms of G6/G7 and the vdW interactions to T5.

DNA Binding Mode of RA-pta. Having observed that RA-en can reach the central G6/G7 bases in the major groove of the 12-mer DNA mainly due to electrostatic interactions, we assumed that the same holds also for RA-pta, since both complexes carry a net charge of 2+. Therefore, the bifunctional $[Ru(\eta^6\text{-arene})(pta)]^{2+}$ moiety (arene = benzene, *p*-cymene) was docked to the adjacent N7 atoms of G6 and G7. In the absence of experimental structural information for the DNA adduct of RA-pta, we started from the crystal structure of the likewise bifunctional cisplatin−DNA adduct[5,34] by exchanging the two compounds. In contrast to the C_2-symmetric cisplatin that binds in only one configuration, RA-pta can potentially bind in two modes that differ by the relative orientation of the arene and pta ligands with respect to the DNA. The pta ligand is either directed toward the backbone of the ruthenated strand with the arene close to the WC hydrogen bonds of the base-pairs (configuration I, Figure 5B) or vice versa (configuration II, Figure S5). Extended classical MD simulations (total of 35 ns) of the *p*-cymene derivative of RA-pta bound to the 12-mer [Cl.6] reveal that binding mode I is favored over II by ∼6 kcal/mol.

In the preferred configuration I, the pta ligand of $[Ru(\eta^6\text{-benzene})(pta)]^{2+}$ remains located between phosphates 6 and 7 during a 15 ps QM/MM MD simulation [Qm.3] (QM region: RA-pta, G6, G7; after 35 ns of MM equilibration [Cl.6]). The pta is solvated by water molecules that form very stable hydrogen bonds to its nitrogen atoms (Figure 5C). One water molecule is highly localized due to a hydrogen bond bridge with a pta nitrogen atom and an oxygen atom of phosphate 7. The RA-pta benzene ring sticks below the methyl group of T5. However, the second coordination to N7(G7) prevents the benzene of RA-pta from inserting between T5 and G6 as deep as in the case of RA-en. Neither the Ru−N7(G) bonds to G6 and G7 nor the Ru−pta bond shows any strain. All of them fluctuate around their unperturbed equilibrium bond distance, and we conclude therefore that the DNA−RA-pta complex is stable in this configuration.

Upon binding, the bifunctional RA-pta induces a local kink at the G6/G7 base step. This behavior is also known for cisplatin and is thought to trigger its anticancer activity.[35] The adjacent guanines G6 and G7, which are parallel in unperturbed B-DNA, roll out of plane to bind the ruthenium center via their N7 atoms. We observed local angles of 21°−24° between the ruthenated GC/GC base-pairs for the different investigated RA-pta derivatives (Table 1). As a consequence, the propeller twist between G6 and C19 is significantly decreased (−25 ± 5° compared to B-DNA = +4°), which weakens the H-bond network between the cDNA strands.

The complex $[Ru(\eta^6\text{-}p\text{-cymene})(pta)]^{2+}$ forms a similar DNA adduct (Figure 5B) [Qm.4]. In contrast to benzene, the *p*-cymene

Table 1. Directed Helix Bending (Angles in Degrees) of DNA Induced by RA Compound Binding

			RA-pta		cisplatin	
	B-DNA	RA-en[a]	benzene	cymene (conf. I)	X-ray[5]	NMR[6]
bending toward major groove	12 ± 10	6 ± 11	42 ± 10	44 ± 10	28	68
bending perpendicular to major groove[b]	−1 ± 9	5 ± 9	4 ± 12	4 ± 11	−9	−22
local G6/G7 step angle[c]	5 ± 2	7 ± 4	21 ± 4	24 ± 4	19	30

[a] Before WC break. [b] Right-handed system: positive angle corresponds to bend in the direction of the ruthenated strand. [c] Local angle between normal vectors of base-pair step (G6-C19)/(G7-C18).

ligand can no longer rotate about its main axis due to its bulky side chains. Moreover, intermittent insertions of its methyl group between T5 and G6 are observed, increasing the corresponding base rise by ∼1 Å compared to B-DNA.

Experimentally, pH-dependent DNA damage has been observed for RA-pta complexes, and it has been speculated that *N*-protonation of the pta ligand might be the reason for this phenomenon.[11] We therefore included [Ru(η^6-benzene)(pta-H$^+$)]$^{3+}$ in our studies.[36] During our classical MD simulation of 20 ns [Cl.5], we identified a very stable H-bond (H−O = 1.86 ± 0.1 Å, N−H−O = 149 ± 6°) between the protonated nitrogen site of the pta ligand and an oxygen atom of phosphate 7 (Figure S7) which is present for 75% of our trajectory.

RA-pta Induces DNA Bending. Due to the slow dynamics of global conformational changes of DNA, we performed extended classical MD simulations (total of ∼120 ns) to allow the DNA to fully adapt to the bound RA complexes [Df.1]. We produced six independent trajectories (three for each arene system, *p*-cymene and benzene) in order to guarantee an acceptable degree of reproducibility of our results. However, since the overall long time configurational changes are very similar in all independent runs, in the following we report on only a single trajectory for each different starting structure.

The highly flexible 12-mer adapts very fast to the perturbation induced by the bound RA complexes and relaxes to a first stable configuration within only 2 ns. The major groove opens significantly around the central G6/G7 pair, but the DNA remains in a B-DNA-like form for the full length of the remaining simulation.

Our results show that the above-reported local angle between G6 and G7 for the bifunctional RA-pta bends the 12-mer globally by more than 40° toward the major groove (Table 1, Figure 6A). We observed very similar global bending angles for RA-pta compounds bearing benzene and *p*-cymene ligands. These results are interesting because the widely used anticancer drug cisplatin is also known to induce a local kink at the DNA binding site upon 1,2-GG intrastrand cross-linking. Recognition of this particular DNA bend is believed to play a crucial role in the mechanism of anticancer activity.[4,35]

In contrast to RA-pta and cisplatin, the RA-en complex does not induce a local kink or a global DNA bending angle. This difference in the global structural changes induced upon DNA binding might explain the different cell responses to the two compounds, RA-en and RA-pta.

For configuration II (Figure S5), we observed a different effect of the RA-pta complexes upon DNA binding. We performed a 22 ns MM and a 4 ps QM/MM MD simulation of the [Ru(η^6-*p*-cymene)(pta)]$^{2+}$−DNA adduct. The propeller twist between G6 and C19 is increased to −37 ± 9°, indicating that the corresponding WC H-bonds are significantly perturbed. The local angle between the central ruthenated GC/GC base-pair amounts again to ∼20° but does not result in a global DNA bend like for RA-pta complexes in configuration I. This is due to the fact that the pta ligand pushes against T5, thereby preventing the formation of a kink toward the major groove (see Table S1). This results in a straight DNA with respect to the direction of the major groove (Figure S6). In contrast, we observe a moderate bending perpendicular to the groove in the direction of the ruthenated strand. This effect is clearly induced by the bulky pta ligand and, in turn, by the arene that forces the DNA to step back.

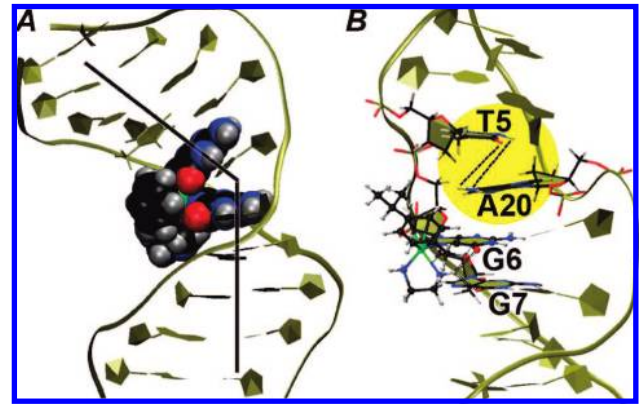

Figure 6. Representative snapshots of the 12-mer DNA upon covalent compound binding. (A) Benzene derivative of RA-pta inducing a global bend toward the major groove (configuration I). (B) RA-en adduct after breaking of the Watson−Crick base-pair T5/A20. The backbone of the ruthenated strand is straightened between T5 and G6, whereas the complementary backbone is compressed around A20, where it shows a "step-like" distortion.

We therefore conclude that not every bifunctional complex that forms 1,2-GG intrastrand cross-link bends DNA globally; this happens only when the nucleobases adjacent to the binding site are allowed to propagate this local kink. Variations in the arene substitution pattern might represent, therefore, an element for rational compound design.

RA-en Binding Induces WC Base-Pair Disruption. As discussed above, the propeller twist between G6 and C19 plays an important role in RA-pta−DNA adducts and perturbs the connecting WC hydrogen bond network significantly. Nevertheless, for RA-pta−DNA adducts, the WC base-pairing is maintained along all our trajectories [Df.1].

In contrast, in the MD simulation of RA-en [Df.2], we observed after ∼14 ns of classical MD simulation of the RA-en−DNA adduct a WC base-pair break next to the bound compound (Figure 6B). As a consequence, the rise between T5 and G6 enlarges to such an extent that A20 can slide in between T5 and G6; thereby, the T5/A20 WC hydrogen bond network is broken but $\pi-\pi$ stacking between T5 and G6 is established. All other WC base-pairs of the dsDNA remain intact. In this way, an additional "base step" is introduced, and within 0.5 ns the 12-mer straightens by 7% (2.5 Å) compared to canonical B-DNA. Similar results were also obtained from two additional MD simulations performed to check the reproducibility of the defect formation starting from different configurations and, in

one case, using a modified force field for the DNA [Df.2c].[52] Our observation is consistent with recent differential pulse polarographic analysis of DNA modified by RA-en.[27] This experiment showed local denaturation of the DNA, suggesting the formation of local single-stranded DNA segments. According to the potential energy from our MM simulations of the system, the denaturated RA-en−DNA adduct is on average 23 kcal/mol more stable than the configuration with unperturbed WC base-pairing. Interestingly, the majority of this energy difference originates from the relaxation of strain accumulated in the dihedral angles of the DNA strands upon compound binding. Entropic arguments also favor the observed WC break. Following the WC base-pair disruption, the volume of the cavity hosting the *p*-cymene enlarges (Figure S8) and allows the thermal activation of its rotational degrees of freedom. On average, however, the cymene prefers a position in which the isopropyl group is oriented toward the backbone of the ruthenated strand (Figure 6B).

QM/MM simulations (10 ps) show that the Ru−N7 bond length remains unaffected by the appearance of the WC break, and the structurally important hydrogen bond between en-N*H1* and O6(G6) is also maintained although weakened (H−O: 2.69 ± 0.28 Å, 116° ± 10°). In contrast, the second H-bond between the same en-N*H1* hydrogen and O6(G7) is strengthened significantly (H−O: 1.98 ± 0.16 Å, 145° ± 11°).

In a final step, we removed the RA-en moiety from its binding site and performed a 30 ns classical MD simulation to study the response of DNA to compound detachment. Our results show that the WC base-pair breaking at T5/A20 is not reversible on this time scale and the dsDNA shows significant unwinding.

Conclusions

Using classical and QM/MM molecular dynamics simulations, we have shown that organometallic ruthenium(II)−arene compounds can bind to the major groove of DNA. Upon binding, the two classes of compounds considered in this study, RA-en and RA-pta, induce different local and global perturbations to the DNA structure.

The monofunctional RA-en complex selectively targets guanine-rich sequences in DNA and is driven to the binding site by electrostatic interactions. Once at binding distance, the amino group of its en moiety forms a characteristic hydrogen bond with the O6 of guanine, while the ruthenium center coordinates to the guanine N7 atom. Moreover, a second H-bond can be formed by the same en-N*H* hydrogen to a second O6 of an adjacent guanine. The resulting RA-en−DNA adduct is 11 kcal/mol more stable than the hydrolyzed RA-en complex. The activation barrier is estimated to be 11 kcal/mol for the binding reaction toward DNA and 21 kcal/mol for the detachment from DNA. The long lifetime of the under-coordinated transition state suggests an interchange or even dissociative mechanism. The cymene ligand of RA-en shows van der Waals interactions with the methyl group of an adjacent thymine and partial intercalation between a guanine and a thymine. The final effect of RA-en binding to DNA is a rupture of a Watson−Crick base-pair at the cymene side of RA-en, causing the DNA to unwind and opening the major groove substantially. This is in agreement with recent experiments and might be the first step toward the observed DNA intercalation of arene ligands with extended π-systems. The local and global changes to DNA differ substantially from those observed for cisplatin, suggesting a different cellular response mechanism.

The bifunctional RA-pta complexes, on the other hand, induce a local kink upon 1,2-GG intrastrand cross-linking. However, the propagation of this local perturbation into the global structure depends on the orientation of the pta ligand. For the energetically favored configuration, and independent of the nature of the arene ligand or the protonation state of pta, a global bending of around 40° of the DNA toward the major groove is observed (cisplatin: X-ray 28°, NMR 68°).

These findings provide important and novel atomistic insights for a detailed understanding of the structural changes in DNA induced upon binding of RA complexes, and it is hoped that they will assist future rational anticancer drug design.

Acknowledgment. We thank Dr. P. Maurer for assistance with the force matching and Dr. G. Wood and Dr. J. S. Arey for comments on the manuscript. Support from the Swiss National Science Foundation is gratefully acknowledged.

Supporting Information Available: Structural details of the QM/MM setup (Figures S1, S2) and further representative snapshots taken from the simulated trajectories (Figures S3−S7); time evolution of the width and depth of the minor and major DNA grooves along the classical dynamics (Figure S8); details about the force field parameters used in the classical and QM/MM setups (Tables S1−S18) and corresponding atomic numbering schemes (Figures S9−S13).This material is available free of charge via the Internet at http://pubs.acs.org.

JA800194A

(52) The same WC break was also observed when the simulations were repeated with an Amber force field with improved dihedral angle parametrization.[37]